A high resolution tidal model for the coast of Møre and Trøndelag, Mid-Norway

HALVARD MOE, BJØRN GJEVIK & ATLE OMMUNDSEN

Moe, H., Gjevik, B. & Ommundsen, A. 2003. A high resolution tidal model for the coast of Møre and Trøndelag, Mid-Norway. *Norsk Geografisk Tidsskrift–Norwegian Journal of Geography* Vol. 57, 65–82. Oslo. ISSN 0029-1951.

A numerical model with grid resolution 500 m has been used to simulate tides on a section of the shelf off the coast of Møre and Trøndelag in western Norway. The model spans c. 3° latitude and covers a sea area of c. $8 \cdot 10^4$ km^2. The fine spatial resolution resolves important fine scale features of the bottom topography on the shelf and the complex coastline with fjords and islands. Boundary conditions at the oceanic sides of the model domain are obtained by interpolation from a larger scale tidal model covering the Nordic Seas. The semi-diurnal components M_2, S_2 and N_2 and the diurnal component K_1 are simulated. Harmonic constants for sea level are compared with observations from 28 stations. The standard deviations between the observed and modeled amplitudes and phases for the dominant semi-diurnal component M_2 are 1.7 cm and 4.8–7.0° respectively. Current fields from the model are compared with measurements from stations along the pipeline from Tjeldbergodden on the coast to the oil and gas fields on the northern rim of Haltenbanken. Parameters, particularly for the M_2 current ellipse, are found to be in good agreement with measurements.

Keywords: *high resolution, Norwegian coast, numerical model, sea level, tidal current, tidal dynamics, tides*

H. Moe, B. Gjevik, A. Ommundsen, Department of Mathematics, University of Oslo, P.O. Box 1053, NO-0316 Blindern, Oslo, Norway. H. Moe is currently affiliated to the Simula Research Laboratory. A. Ommundsen is currently affiliated to the Norwegian Defence Research Establishment. E-mail: bjorng@math.uio.no

Introduction

The continental shelf outside Møre and Trøndelag on the western coast of Norway is only c. 70 km wide west of Ålesund while the width increases northward to c. 230 km west of Rørvik (Figs. 1 and 2). Several banks are located on this section of the shelf. The largest is Haltenbanken, with its central shallow part located c. 100 km south-west of Rørvik and depths of c. 100 m. Along the shelf edge flows a strong branch of the Norwegian Atlantic Current (Mathisen 1998, Orvik et al. 2001). On the shelf the current is generally weaker, with topographically trapped anticyclonic eddies over the banks (Eide 1979, Haugan et al. 1991, Gjevik & Moe 1994). Near the coast, current speed is higher due to the Norwegian coastal current. These features are also clearly revealed by experiments with Lagrangian drifters (Poulain et al. 1996, Sætre 1999). The favorable circulation pattern and supply of nutritients make the banks important spawning grounds for herring, coalfish (pollock) and other commercially important fish stocks. Exploration for oil and gas started in this area in c. 1985. Today, several production fields are in operation around Haltenbanken, notably the Draugen (Fig. 2, map code 6), Heidrun (20 km west of map code 35) and Midgard (near map code 7) fields. Exploration has now moved into deeper water, with plans for production in the Ormen Lange field on the shelf slope c. 130 km west of Kristiansund. Pipelines for oil and gas are constructed from the Heidrun and Aasgard fields on the northern rim of Haltenbanken to the refinery plant at Tjeldbergodden (near map code 29). For these reasons there has been a considerable interest in studying current, waves and other metocean conditions in this area of the Norwegian shelf. Several field measurement programs have been conducted, funded mostly by the oil industry. Only some of the results from these studies are published in scientific journals, while for the most part the results are available in project and institute reports, which are often difficult to obtain.

The tide is an important part of the current variability in

Fig. 1. Map of the Norwegian continental shelf with depth contours (meters) and model domain (rectangular box).

DOI 10.1080/00291950310001522

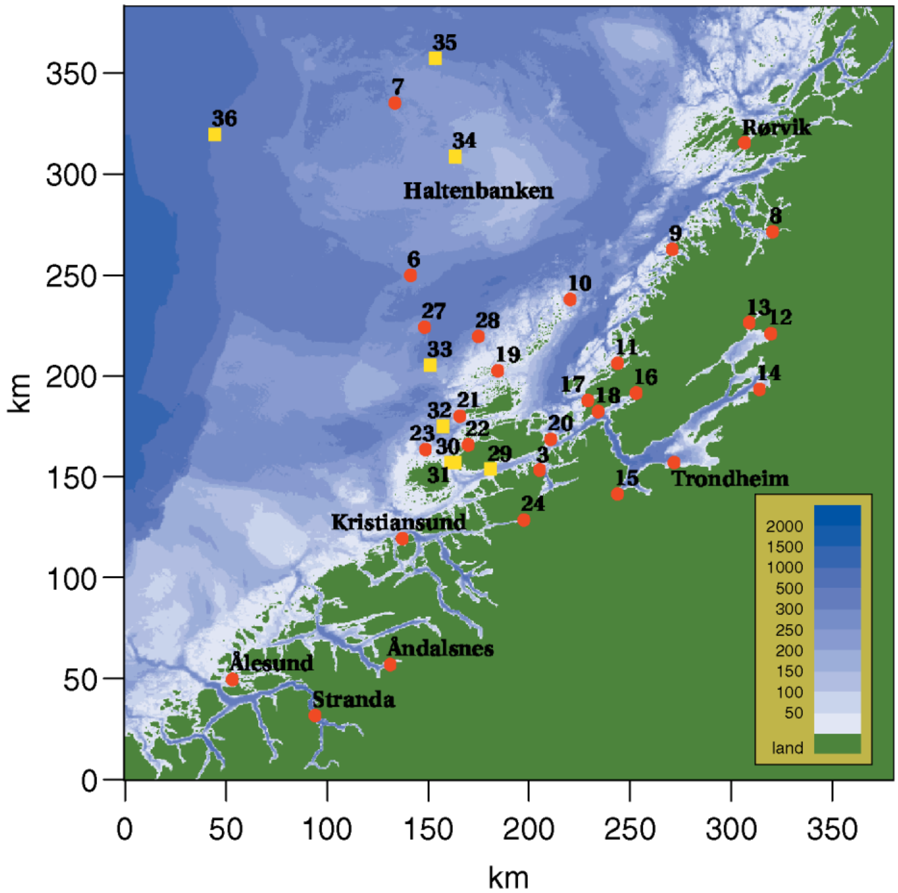

Fig. 2. Model domain with 0.5 km grid resolution. Color depth-scale in meters. The positions of the tidal stations, above the line in Table 2, are marked with red dots and corresponding map codes. The yellow squares indicate stations with only current measurements (below the line in Table 2).

this area, particularly in the coastal zone, and has previously been modeled with relatively coarse grid models covering the adjacent deep sea (Gjevik 1990), and a local model with refined grid resolution (Nøst 1988). Gjevik et al. (1992) implemented a high resolution model with grid size 0.5 km for this area for the Norwegian oil company, *Statoil*. The report by Gjevik et al. (1992) published the results of the model simulations and comparison with sea level and current measurements along the track of the pipeline between Tjeldbergodden and Heidrun. The model area (Fig. 2) in this study is extended and the boundary conditions for the model are upgraded. The new model covers a sea area of c. $8 \cdot 10^4$ km^2, spanning from the shelf edge to the inner fjords, with a grid resolution of 0.5 km. Both the important topographic features of banks and trenches on the shelf and the fjords and channels between islands are resolved by this model. Simulations are performed for the main semi-diurnal components M_2, S_2 and N_2 and the diurnal component K_1 (see section on model equations below). The results are compared with sea level observations from 28 stations and current observations from 12 stations (Fig. 2). Most of the latter are located along the track of the pipeline between Haltenbanken and Tjeldbergodden.

Three large islands are located at the coast in the center of the model domain: Hitra (between map codes 20 and 22), Smøla (near map code 31) and Frøya (east of map code 21). A chain of small islands, Froan, stretches north-eastward from Frøya towards Halten (map codes 10–19). Between this chain of islands and the mainland is a deep ocean bay, Frohavet, cutting inwards towards the entrance to Trondheimsfjorden, named after the city of Trondheim. This system of islands with sounds and channels in between has an important effect on the tide in the area.

High resolution tidal modeling for shelf and coastal areas with complex bathymetry and coastlines is a challenging and rapidly developing subject. A review of the state of the art is given by Davies et al. (1997a, 1997b). In particular, the treatment of strong non-linear effects, such as turbulence, flow separation and eddy formation, is a difficult task which requires special precautions (Maddock & Pingree 1978, Geyer 1993). Although this model study aims specifically towards an understanding of the dynamics of the tides in the Haltenbanken area many of the problems encountered here are of wider interest.

For example, a similar high resolution model to the one used in this study has recently been developed for the Lofoten area in northern Norway (Moe et al. 2002).

Model equations

The depth-integrated shallow water equations are formulated in flux form in a Cartesian coordinate system (x, y, z) with the x and y axis in the horizontal plane and the z axis vertical:

$$\frac{\partial U}{\partial t}+\frac{\partial}{\partial x}(\frac{U^2}{H})+\frac{\partial}{\partial y}(\frac{UV}{H})-fV=$$

$$-gH\frac{\partial\eta}{\partial x}-c_D\frac{\sqrt{U^2+V^2}}{H}\frac{U}{H} \tag{1}$$

$$\frac{\partial V}{\partial t}+\frac{\partial}{\partial x}(\frac{UV}{H})+\frac{\partial}{\partial y}(\frac{V^2}{H})+fU=$$

$$-gH\frac{\partial\eta}{\partial y}-c_D\frac{\sqrt{U^2+V^2}}{H}\frac{V}{H} \tag{2}$$

where (U, V) specify the components of volume flux vector per unit length in the horizontal plane, η the vertical displacement of the sea surface from the mean sea level, $H = H_0 + \eta$ the total depth, H_0 the mean depth, g acceleration of gravity, f the Coriolis parameter, and c_D the drag coefficient of the quadratic bottom shear stress. In addition, the continuity equation reads:

$$\frac{\partial\eta}{\partial t}=-\frac{\partial U}{\partial x}-\frac{\partial V}{\partial y} \tag{3}$$

The depth mean current velocity is defined by:

$$\bar{u}=\frac{U}{H},\bar{v}=\frac{V}{H}$$

In this model domain the direct effect of the tide-generating forces is negligible, and the tidal motion is mainly driven by the boundary input, i.e. sea surface elevation and volume fluxes. For models covering large domains, the tide-generating force is known to be important for the diurnal tidal components (Gjevik & Straume 1989, Davies et al. 1997c). In the present problem, these equations span a wide parameter range from weak tidal flows on the deeper part of the shelf to strong tidal currents at the coast. A velocity scale u_s, a time scale t_s corresponding to half the tidal period, a tidal amplitude a, a length scale for the spatial variation of the tidal flow l_s, and a depth scale h_s are introduced. With this scaling the tidal excursion is defined $l_t = u_s t_s$ and the equations (1)-(2) can be recast into dimensionless form:

$$\frac{\partial U}{\partial t}+\alpha[\frac{\partial}{\partial x}(\frac{U^2}{H})+\frac{\partial}{\partial y}(\frac{UV}{H})]-\delta V=$$

$$-\beta H\frac{\partial\eta}{\partial x}-\gamma\frac{\sqrt{U^2+V^2}}{H}\frac{U}{H} \tag{4}$$

$$\frac{\partial V}{\partial t}+\alpha[\frac{\partial}{\partial x}(\frac{UV}{H})+\frac{\partial}{\partial y}(\frac{V^2}{H})]+\delta U=$$

$$-\beta H\frac{\partial\eta}{\partial y}-\gamma\frac{\sqrt{U^2+V^2}}{H}\frac{V}{H} \tag{5}$$

The dimensionless form of the continuity equation reads:

$$\frac{\varepsilon}{\alpha}\frac{\partial\eta}{\partial t}=-\frac{\partial U}{\partial x}-\frac{\partial V}{\partial y} \tag{6}$$

with $H = H_0 + \varepsilon\eta$. The same symbols are here tacitly used for dimensionless variables U, V, H and η as in the dimensional equations (1)-(3). The dimensionless parameters are defined by:

$$\alpha=\frac{l_t}{l_s},\beta=\frac{gal_t}{{u_s}^2l_s},\gamma=\frac{c_Dl_t}{h_s},\delta=ft_s,\varepsilon=\frac{a}{h_s} \tag{7}$$

Here, α and ε are measures of the importance of the convective terms and the non-linear surface elevation terms, respectively. The parameters β, γ and δ scale pressure, bottom friction and rotational effects, respectively. In deep water α, ε and $\gamma \ll 1$ reducing the equations to the linearized shallow water equation with negligible bottom friction. Near the coast, with strong tidal currents, α, β, γ are of order one (O (1)) and all terms in the equation of motion have to be retained. In not too shallow water $\varepsilon \ll 1$, the left-hand side of equation (3) may be neglected, rendering a nearly non-divergent volume flux as long as α is of O (1).

In this paper, the performance of a linear tidal model has been tested and the approximations $\alpha = \varepsilon = 0$ and ε/α of O (1) have been made. The equations are then discretised on a C-grid (Mesinger & Arakawa 1976), with a semi-implicit numerical scheme. This scheme is widely used for depth-integrated ocean models. A discussion of its dispersion and stability properties is given, for example, by Martinsen et al. (1979) and Gjevik & Straume (1989).

The stability criterion satisified by the numerical time step Δt is:

$$\Delta t \leq \frac{\Delta x}{2\sqrt{2gH_{max}}},$$

where Δx is the grid size and $H_{\max}$ is the maximum depth in the model domain.

The tidal motion is assumed to be a superposition of harmonic components. For the sea surface displacement this can be written:

$$\eta(x,y,t)=\sum_n h_n\cos(\omega_n t+\chi_n-g_n) \tag{8}$$

where ω_n is the angular velocity, the corresponding period $T_n = 2\pi / \omega_n$, h_n and g_n are the harmonic constants, amplitude and phase respectively. These are functions of x and y; $h_n = h_n\ (x, y)$ and $g_n = g_n\ (x, y)$. The phase function χ_n is the astronomic argument which is determined by the position of the sun and the moon (Schwiderski 1980, Gjevik et al. 1990). When the harmonics constants are determined, either from measurements or from modeling, the time series for the sea surface displacement can be calculated from equation (8). A similar harmonic decomposition can be made for the components of the mean current speed:

$$\bar{u}(x,y,t)=\sum_n \bar{u}_n\cos(\omega_n t+\chi_n-g_n^u)$$

$$\bar{v}(x,y,t)=\sum_n \bar{v}_n\cos(\omega_n t+\chi_n-g_n^v)$$

where $\bar{u}_n$, $\bar{v}_n$ and ${g^u}_n$, ${g^v}_n$ are the respective harmonic constants for the current components. It can be shown that the current vector for each harmonic component describes an ellipse, called the tidal current ellipse. The major and minor half axes of the ellipse are denoted A and B, respectively, and the orientation of the major axis (θ) can be calculated from

Table 1. List of major harmonic components.

Symbol	*Period* (T_n) *hours*	*Frequency* (ω_n) 10^{-4}rad/s	*Description*
M_2	12.42	1.40519	Principal lunar, semi-diurnal
S_2	12.00	1.45444	Principal solar, semi-diurnal
N_2	12.66	1.37880	Elliptical lunar, sem-idiurnal
K_1	23.93	0.72921	Declinational luni-solar, diurnal

the harmonic constants for the current components (Foreman 1978). In this paper we limit the study to the three major semi-diurnal components M_2, S_2 and N_2 and the diurnal component K_1 (Table 1).

Model set-up and boundary conditions

The depth matrix was evaluated on a UTM coordinate grid with $\Delta x = 0.5$ km resolution. Near the coast, average depths for each grid cell were read from regular Norwegian coastal sea charts at scale 1:50,000. Outside the zone covered by the charts depths are taken from a bathymetric database with 500 m spatial resolution (Norwegian Hydrographic Service (NHS) 1992). Based on the resulting depth matrix of 761×767 grid points, the color contour depth map is produced (Fig. 2).

Boundary conditions for the model were obtained by interpolating harmonic constants for surface elevation and volume fluxes from a larger scale model of the Norwegian Sea and the Barents Sea with 25 km grid resolution (Gjevik et al. 1990, 1994). The flow relaxation scheme (FRS), (Martinsen & Engedahl 1987), has been used to impose the boundary conditions. The rationale behind this scheme is to soften the transition from an exterior solution (here, the interpolated data) to an interior solution (model area) by use of a grid zone where the two solutions dominate at each end respectively. The width of the zone is taken to be 10 grid cells.

Two types of boundary forcing (exterior solutions) have been tested: i) only surface elevation specified, ii) both surface and and volume fluxes specified. Separate simulations were made for each of the tidal components M_2, S_2, N_2 and K_1. At $t = 0$ the boundary forcing is applied from rest at the oceanic sides of the model domain and the amplitudes grow according to $(1 - \exp(-\sigma t))$. A value of $\sigma = 4.6 \cdot 10^{-5}\ \mathrm{s}^{-1}$ has been used which implies full effect of boundary conditions after c. 12 hours. The simulations are started from rest, i.e. initially the internal solution $U = V = \eta = 0$. The simulation times are taken to be 192 hours for the semi-diurnal components and 240 hours for the diurnal component. Entire fields (all grid points) for current and elevation are stored for one tidal period at one-hour intervals for each component at the end of the simulations, while for 45 stations within the model area records are kept with three minutes sampling for the whole simulation interval. The time series for the stations have been used to ensure that a steady state oscillation is reached. Harmonic analysis is performed on the entire fields and on the time series of the stations yielding harmonic constants for amplitude and phase, both for sea surface elevation and current. From the latter, the parameters of the current ellipse are calculated.

Table 2. List of stations.

Station	*Coordinates*	*Map Code*
Rørvik	64°52′N, 11°15′E	Rørvik (1)
Trondheim	63°26′N, 10°26′E	Trondheim (2)
Heimsjø	63°26′N, 09°07′E	3
Kristiansund	63°07′N, 07°45′E	Kristiansund (4)
Ålesund	62°28′N, 06°09′E	Ålesund (5)
Draugen	64°17′N, 07°47′E	6
Haltenbanken 1	65°03′N, 07°35′E	7
Namsos	64°28′N, 11°30′E	8
Buholmråsa	64°24′N, 10°28′E	9
Halten	64°11′N, 09°25′E	10
Lysøysundet	63°53′N, 09°52′E	11
Steinkjer	64°02′N, 11°30′E	12
Malm	64°05′N, 11°14′E	13
Levanger	63°45′N, 11°18′E	14
Orkanger	63°19′N, 09°52′E	15
Råkvåg	63°46′N, 10°04′E	16
Uthaug	63°44′N, 09°35′E	17
Brekstad	63°41′N, 09°40′E	18
Mausundvær	63°52′N, 08°40′E	19
Hestvika	63°34′N, 09°12′E	20
Titran	63°40′N, 08°19′E	21
Kvenvær	63°32′N, 08°23′E	22
Veidholmen	63°31′N, 07°58′E	23
Vinjeøra	63°13′N, 08°59′E	24
Åndalsnes	62°33′N, 07°40′E	Åndalsnes (25)
Stranda	62°19′N, 06°57′E	Stranda (26)
St15	64°04′N, 07°57′E	27
St16	64°39′N, 07°43′E	28
St04	63°26′N, 08°37′E	29
St07	63°27′N, 08°13′E	30
St09	63°32′N, 08°15′E	31
St11	63°37′N, 08°08′E	32
St13	63°53′N, 08°00′E	33
Haltenbanken 2	64°49′N, 08°13′E	34
Haltenbanken 3	65°15′N, 08°00′E	35
Helland Hansen	64°53′N, 05°43′E	36

Most of the simulations have been made including bottom friction (coefficient $c_D = 0.003$), however, runs without friction were also performed for comparison. The fields presented in the Figures in this paper are all from simulations with bottom friction and with only surface elevation as the exterior solution.

Results and discussion

The calculated harmonic constants for sea level amplitude h_n and phase g_n relative Greenwich time (GMT), are compared with observations from 28 tidal stations (above the line in Table 2). In this article mainly the results for the dominant semi-diurnal tidal component M_2 and the diurnal component K_1 will be presented. The amplitudes of the other two semi-diurnal components included in the simulations, S_2 and N_2, are only about one-third and one-fifth of the amplitude of the M_2 component respectively. Also, the general pattern of amplitude and phase variation for these smaller components is found to resemble the M_2 component. The regression

Table 3. Harmonic constants for sea level (M_2). Amplitude (h_n) in cm, phase (g_n) in degrees (GMT). Measured and derived results in columns 2–5. Model results with only elevation, and both flux and elevation as exterior solution in columns 6–9. The latter also without bottom friction in columns 10–11.

	Observed		*Derived*		*Elevation*		*Elevation & Flux*		*Without Friction*	
Station	h_n	g_n	h_n	g_n	h_n	g_n	h_n	g_n	h_n	g_n
Rørvik	78.8	309			78.8	306	79.6	307	79.6	307
Trondheim	92.3	306			90.9	299	92.7	300	92.5	300
Heimsjø	77.8	301			77.1	297	78.7	298	78.7	297
Kristiansund	67.7	295			68.2	292	69.9	293	69.9	293
Ålesund	61.8	290			62.6	288	65.3	289	65.3	289
Draugen	67.3	304			67.0	300	68.3	300	68.2	300
Haltenbanken 1	67.7	344			65.1	305	66.0	306	66.0	306
Namsos	75.9	306	77.2	304	78.9	304	80.2	305	80.2	305
Buholmråsa			78.0	302	76.4	303	77.7	304	77.8	304
Halten	74.8	303	75.6	306	74.4	301	75.8	302	75.6	302
Lysøysundet	76.6	307	77.2	305	76.4	301	77.9	302	77.9	302
Steinkjer	96.9	307	101.5	305	98.8	300	100.7	301	100.4	300
Malm	97.1	306	105.2	305	99.2	300	101.2	301	100.9	300
Levanger	98.0	309	98.8	311	95.2	300	97.1	301	96.8	300
Orkanger	87.4	306	94.1	308	89.9	300	91.7	300	91.4	300
Råkvåg	86.3	302	86.8	297	85.3	300	87.0	301	86.8	300
Uthaug	76.7	305	76.5	300	77.6	300	79.0	301	79.1	301
Brekstad	82.9	307	86.7	307	84.4	300	86.1	301	85.9	300
Mausundvær	73.2	305	73.8	295	73.2	298	74.7	299	74.9	298
Hestvika	77.7	307	79.9	305	78.7	299	80.2	300	80.3	299
Titran	69.7	292	68.4	293	69.0	296	70.5	296	70.5	296
Kvenvær			68.4	296	69.7	295	71.2	296	71.2	296
Veidholmen	67.4	297	69.1	291	68.8	294	70.3	295	70.4	295
Vinjeøra			74.5	292	71.8	293	73.5	294	73.4	294
Åndalsnes	65.6	290	65.7	286	67.4	290	69.9	291	69.7	291
Stranda	62.5	293	62.3	284	64.1	288	66.9	289	67.0	289
St15	68.3	300			67.9	298	69.3	299	69.2	299
St16	66.5	304			70.5	298	71.9	299	71.9	299

Table 4. Harmonic constants for sea level (K_1). Amplitude (h_n) in cm, phase (g_n) in degrees (GMT). Measured and derived results in columns 2–5. Model results with only elevation, and both flux and elevation as exterior solution in columns 6–9. The latter also without bottom friction in columns 10–11.

	Observed		*Derived*		*Elevation*		*Elevation & Flux*		*Without Friction*	
Station	h_n	g_n	h_n	g_n	h_n	g_n	h_n	g_n	h_n	g_n
Rørvik	7.4	168			9.3	164	9.2	166	9.2	166
Trondheim	6.7	166			8.7	159	9.0	162	9.0	162
Heimsjø	6.3	165			8.2	159	8.4	161	8.4	161
Kristiansund	6.0	167			7.5	158	7.9	161	7.9	161
Ålesund	5.9	153			7.1	155	7.9	157	7.9	157
Draugen	6.8	170			8.2	165	8.3	167	8.3	167
Haltenbanken 1	6.7	201			8.1	174	8.0	173	8.0	173
Namsos	6.4	172	7.3	165	9.0	162	9.1	165	9.1	165
Buholmråsa			7.3	164	8.9	162	9.0	164	9.0	164
Halten	7.8	162	7.1	166	8.5	162	8.8	164	8.8	164
Lysøysundet	5.8	163	7.3	166	8.5	160	8.8	163	8.8	163
Steinkjer	7.1	175	7.4	165	8.8	159	9.2	162	9.2	162
Malm	6.5	174	7.6	165	8.8	159	9.2	162	9.2	162
Levanger	6.5	156	7.2	168	8.8	159	9.1	162	9.1	162
Orkanger	4.8	182	6.8	167	8.7	159	9.0	162	9.0	162
Råkvåg	6.5	158	6.3	161	8.6	160	8.9	162	8.9	162
Uthaug	6.5	175	6.8	170	8.4	160	8.7	162	8.7	162
Brekstad	7.8	156	7.7	173	8.6	160	8.9	162	8.9	162
Mausundvær	6.3	164	6.5	167	8.2	160	8.4	162	8.4	162
Hestvika	6.5	164	7.1	172	8.4	160	8.7	162	8.7	162
Titran	5.9	152	6.1	166	7.9	159	8.2	161	8.2	161
Kvenvær			6.1	168	7.9	159	8.2	161	8.2	161
Veidholmen	5.9	160	6.1	165	7.9	158	8.1	160	8.1	160
Vinjeøra			6.6	165	7.8	158	8.1	161	8.1	161
Åndalsnes	7.9	178	5.8	162	7.5	158	8.0	161	8.0	161
Stranda	5.8	149	5.5	161	7.2	155	7.9	157	7.9	157
St15	6.0	149			8.1	162	8.3	164	8.3	164
St16	6.7	157			8.3	160	8.6	162	8.6	162

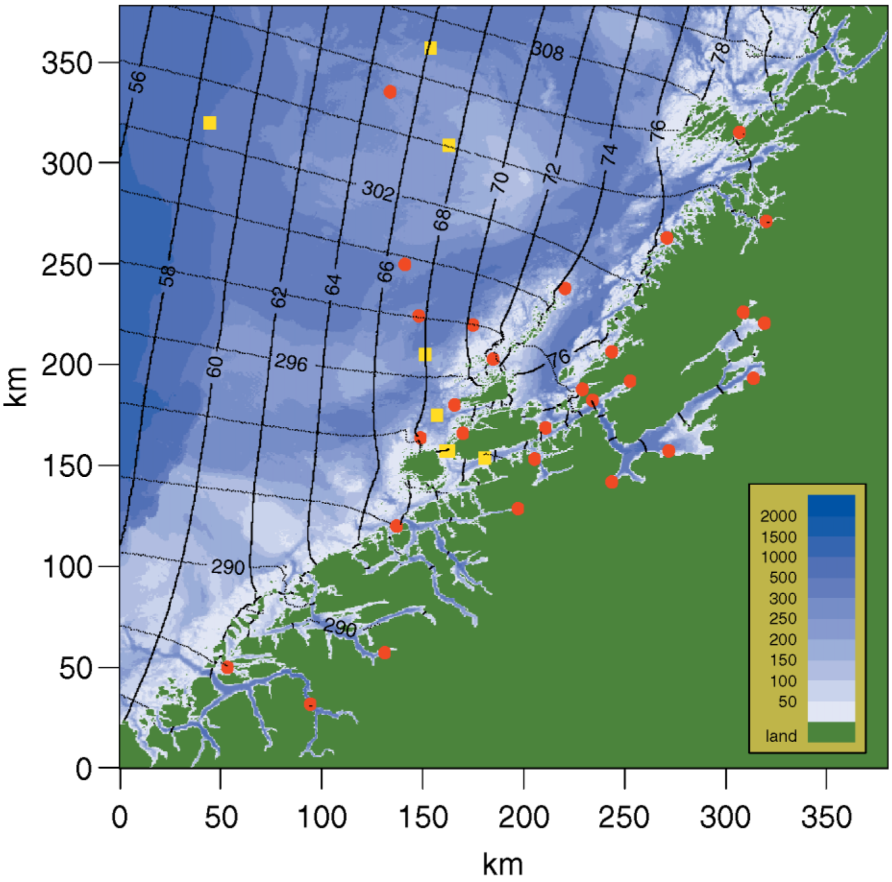

Fig. 3. Simulated M_2 sea surface elevation. Isolines for amplitude (h_n) with 2-cm intervals (solid lines) and for phase (g_n) with 2° intervals (broken lines). Shading shows depth with scale in legend (meters). Stations are marked as in Fig. 2.

analysis for S_2 and N_2 show that these components can be simulated with the same high accuracy as M_2 (see section on the M_2 component below). Further results for S_2 and N_2 can be found in Moe et al. (2000).

For Rørvik, Trondheim, Heimsjø, Kristiansund and Ålesund (primary stations), the harmonic constants are calculated from long time series of observed sea level (Norwegian Hydrographic Service 2000). For the other tidal

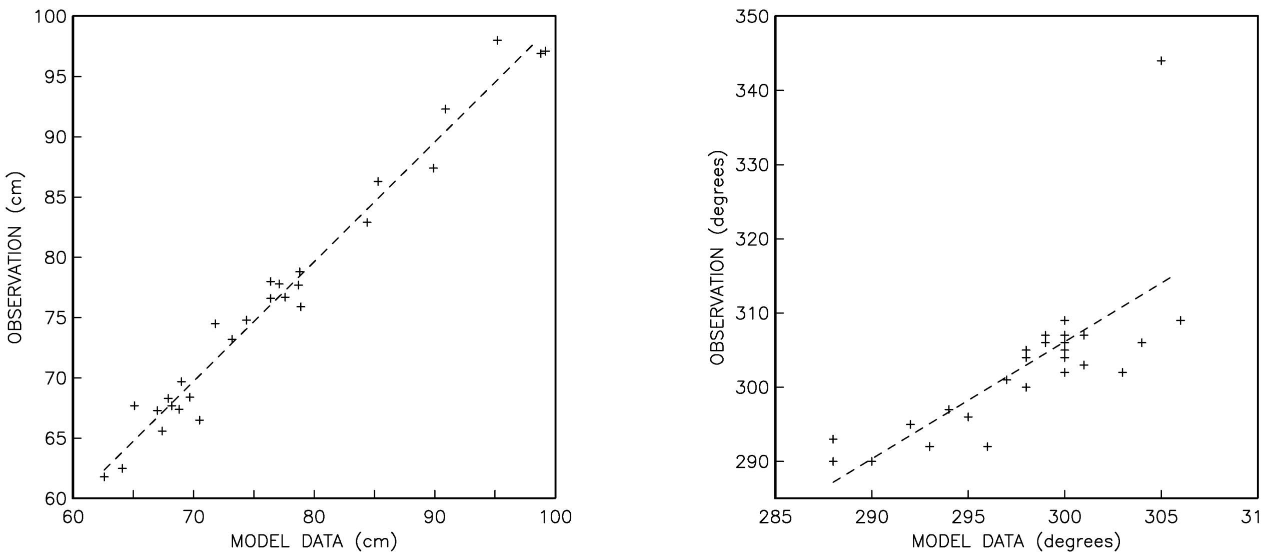

Fig. 4. Scatter diagrams for M_2. Comparison between modeled and observed amplitude (left panel) and phase (right panel), for the elevation run (all 28 stations). The least squares regression line (dashed). The standard deviation estimate between model and observation is 1.7 cm (amplitude) and 7.0° (phase). The explained variance R^2 is 97.3% for amplitude and 53.5% for phase.

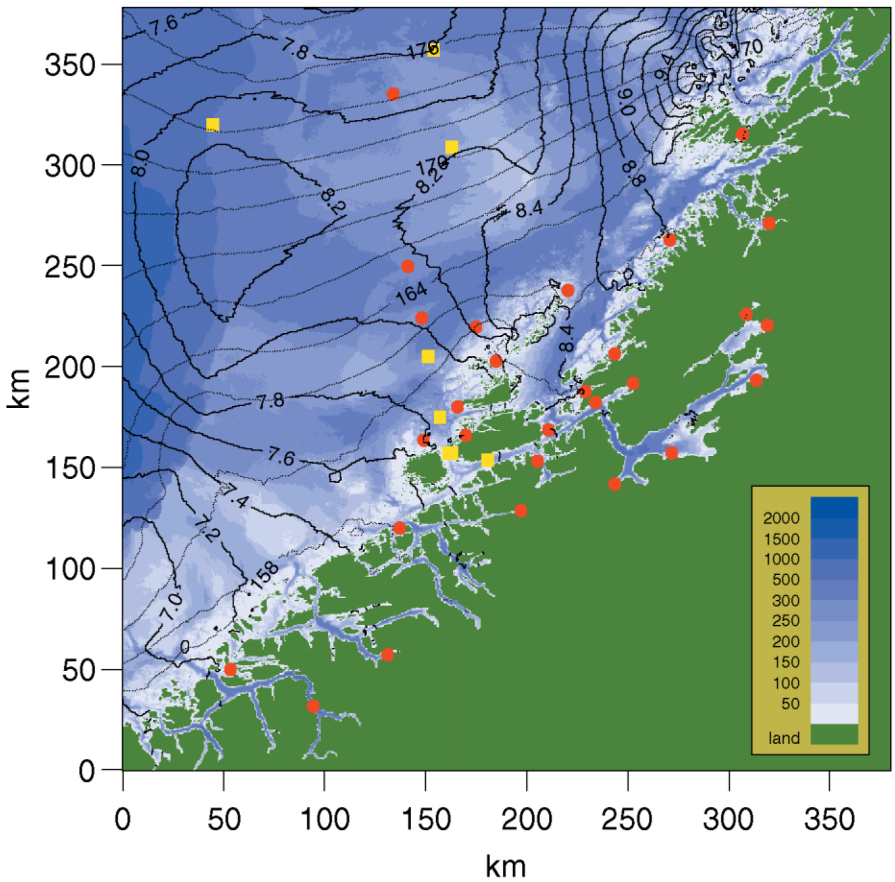

Fig. 5. Simulated K_1 sea surface elevation. Isolines for amplitude (h_n) with 0.2-cm intervals (solid lines) and for phase (g_n) with 2° intervals (broken lines). Shading shows depth with scale in legend (meters). Stations are marked as in Fig. 2.

stations in Table 2, except for Buholmråsa, Kvenvær and Vinjeøra, the harmonic constants for M_2 and K_1 are calculated from shorter time series, typically 2–4 weeks. Access to this data set, which previously has not been used for validation of tidal models, was given by the Norwegian Hydrographic Service (NHS). For some of the stations (secondary stations), the NHS has also calculated correction factors for amplitude and time of high and low water relative

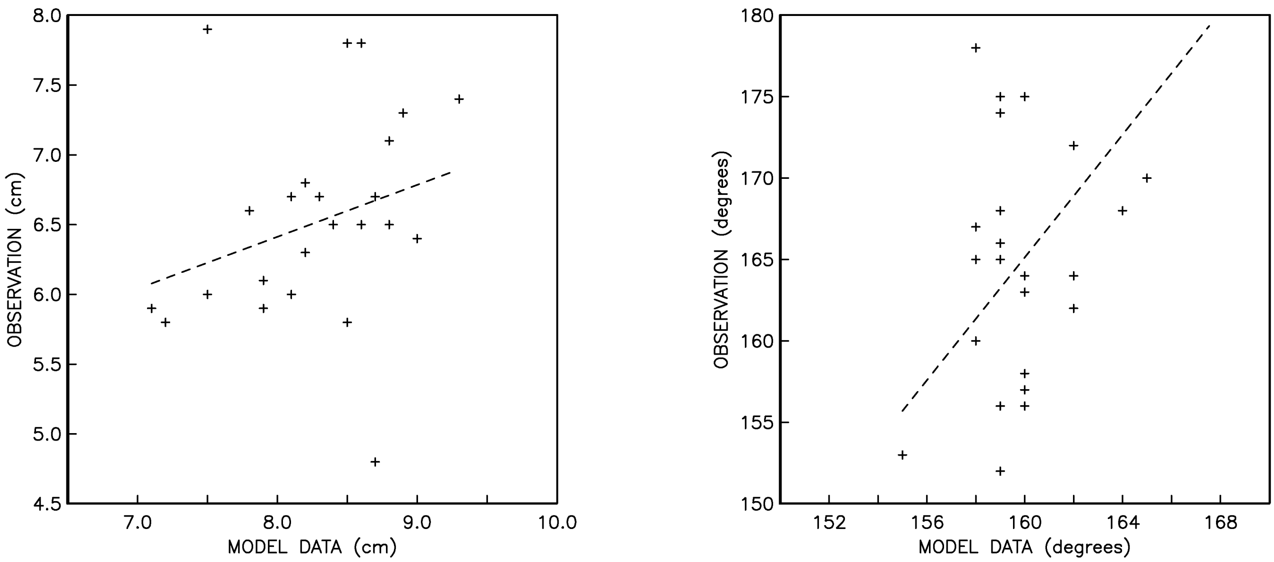

Fig. 6. Scatter diagrams for K_1. Comparison between modeled and observed amplitude (left panel) and phase (right panel), for the elevation run (all 28 stations). The least squares regression line (dashed). The standard deviation estimate between model and observation is 1.9 cm (amplitude) and 10.6° (phase). The explained variance, R^2 is 8.4% for amplitude and 35.5% for phase.

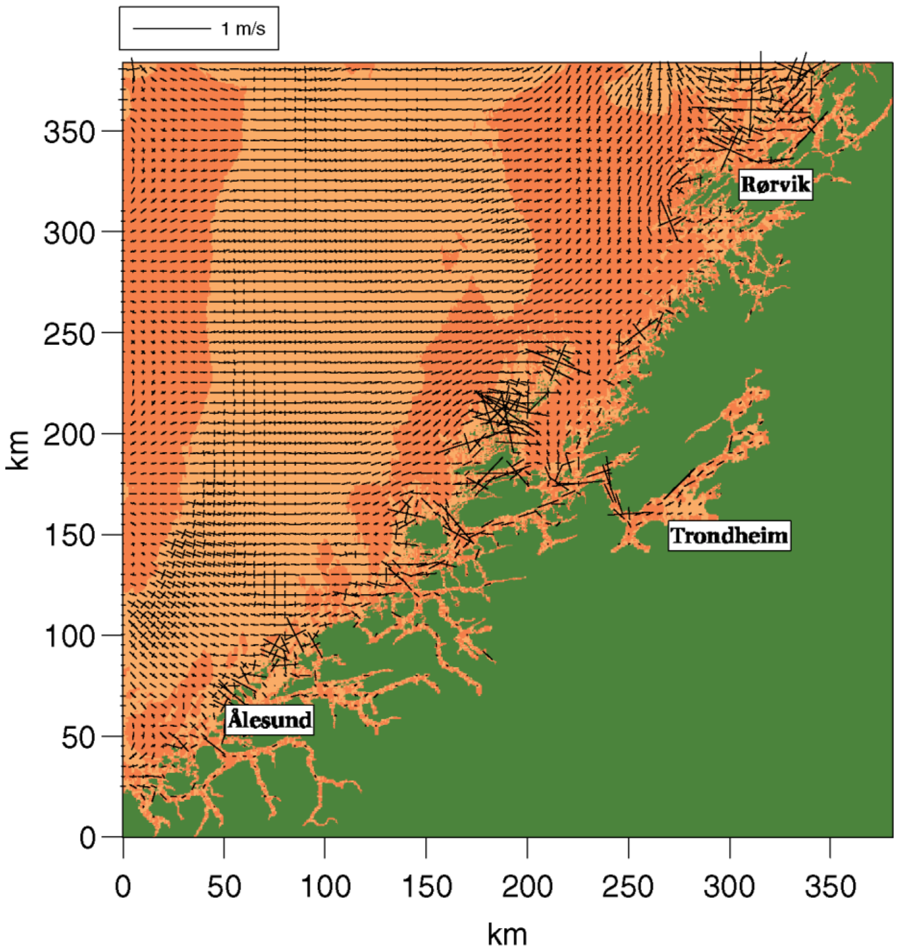

Fig. 7. Tidal ellipse and rotation of the M_2 current vector. Bright shadowing clockwise rotation, darker shadowing counterclockwise. The crosses show the major and minor axes.

to the nearest primary station. By using these correction factors, a set of derived harmonic constants for the secondary stations has been deduced. Harmonic constants for both primary and secondary stations as well as model estimates are listed in Tables 3 and 4. Observed phases at the station Haltenbanken 1 (map code 7) are somewhat odd. It deviates 39° from the model for the M_2 component (about one hour) and 26° for the diurnal component (almost two hours). Compared to the good agreement between modeled and observed phases of other neighboring stations we believe that the timing or the processing of the data from this station is erroneous. Since we have not been able to confirm this hypothesis we have retained the station in the regression analysis. This should be kept in mind when looking at the regression plots in Figs. 4 and 6. If the station is excluded (see section on the M_2 component below), the explained variance improves substantially, particularly for the M_2 phase.

Current data from the model is compared with observational data along the Tjeldbergodden pipeline, provided by *Statoil* and *Oceanor*. Where data from several depths were available, the mean value was used for comparison. For near-bottom measurements we have assumed a boundary layer profile to calculate a representative mean value. This is discussed further in the section on Ramsøyfjorden below.

Sea level, semi-diurnal and diurnal components

The M_2 component. Contour lines for the M_2 sea level amplitude and phase are shown in Fig. 3. The phase lines are approximately perpendicular to the shelf edge, with gradually increasing phases north-north-eastward, showing that the M_2 wave component propagates basically in a north-north-eastward direction. Note that a 2° increase in phase corresponds to about a 4 minutes time delay of the tide. The separation between phase lines is larger in the southern part of the model area where the shelf is narrow, which implies a larger propagation speed than in north where the shelf is wider.

By comparing amplitudes and phases with observations (Table 3), the best fit is found for the run, with prescribed surface elevation at the open boundaries, with a standard deviation of 1.7 cm for amplitude and 7.0° for phase, and with all 28 stations included (Fig. 4). The explained variance R^2 is 97.3% for amplitude and 53.5% for phase. By disregarding the station Haltenbanken 1 (see section on results and discussion above), the standard deviation is reduced to 4.8°, with an explained variance of 75.2% for phase.

The difference between the three-model simulation (Table 3) is not substantial even though including flux generally

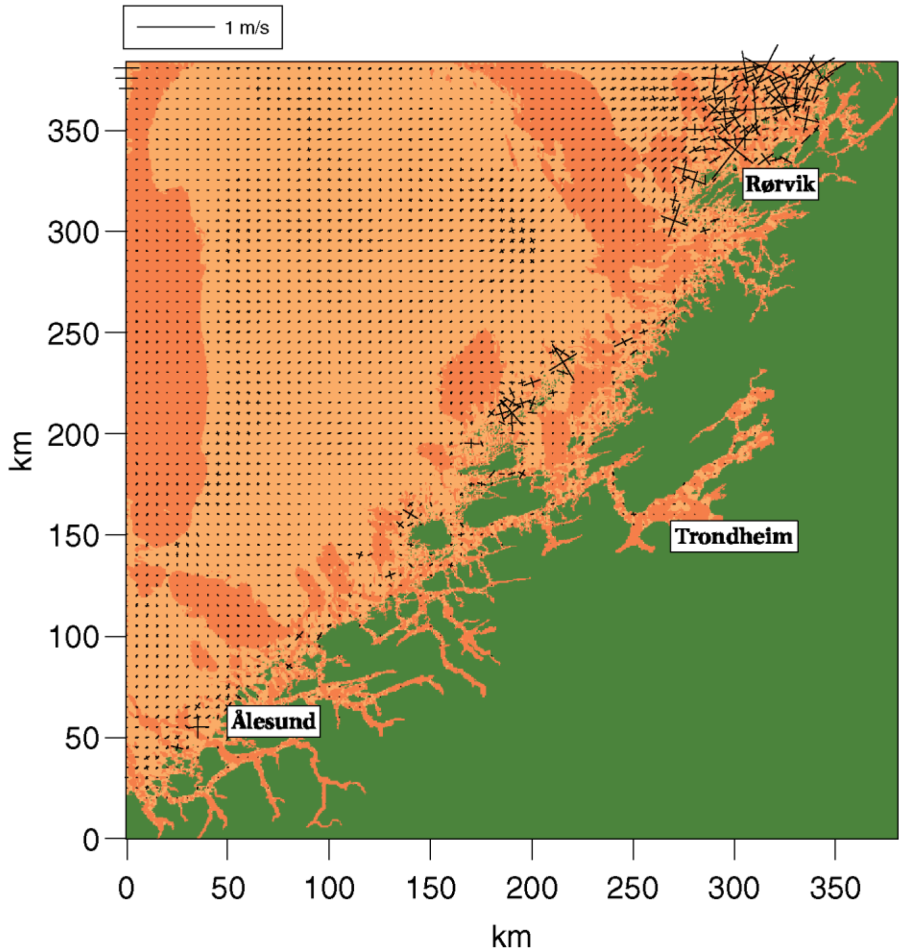

Fig. 8. Tidal ellipse and rotation of the K_1 current vector. Bright shadowing clockwise rotation, darker shadowing counterclockwise. The crosses show the major and minor axes.

gives a higher amplitude. Inward the Trondheimsfjord an increase in amplitude is seen in good agreement with measurements (Table 3).

The K_1 component. The amplitude of sea surface displacement for the largest diurnal component, K_1, is small compared to M_2. The contour lines for amplitude and phase are shown in Fig. 5. The ratio between the K_1 and M_2 major axis is plotted (Fig. 9) and shows that in some areas, for example outer Sunnmøre and the Froan area, the K_1 current dominates. This is discussed further in the section on tidal current below.

The regression analysis between observed and model amplitude and phase shows a relatively large scatter, particularly for phase (Fig. 6). Standard deviation is 1.9 cm for amplitude and 10.6° for phase. The explained variance R^2 is only 8.4% for amplitude and 35.5% for phase. The large scattering shows that it is a much more difficult task to simulate the diurnal component K_1 with a similar high degree of relative accuracy as obtained for the semi-diurnal components. One reason for this is that K_1 is more influenced by local topographic features due to possible resonance with shelf wave modes (see section on Outer Sunnmøre below). An optimalization of the K_1 solution is therefore a challenge for future simulation efforts.

The modeled amplitudes are generally 20–30% higher than observed. To compensate for this, a heuristic optimalization by reducing the amplitude of the exterior solution by 20% was performed. This made amplitudes fit the observed much better (standard deviation is 0.7 cm), and shows that much can be gained by systematically utilizing optimizing techniques and probably also by refining the exterior solutions, i.e. the input of the model.

Tidal current

Figs. 7 and 8 show the M_2 and K_1 current ellipses and current vector rotation for the simulation area. The model predicts relatively weak currents on the shelf and stronger currents in the shallow areas along the coast for both components. For most parts, the M_2 current is the larger, but the K_1 dominates for some small areas (Fig. 9). We do not know of any available observational data which may confirm these findings, and this could therefore be an interesting task to test for future measurements. In the area north of Rørvik there are large currents for both M_2 and K_1. Since this is close

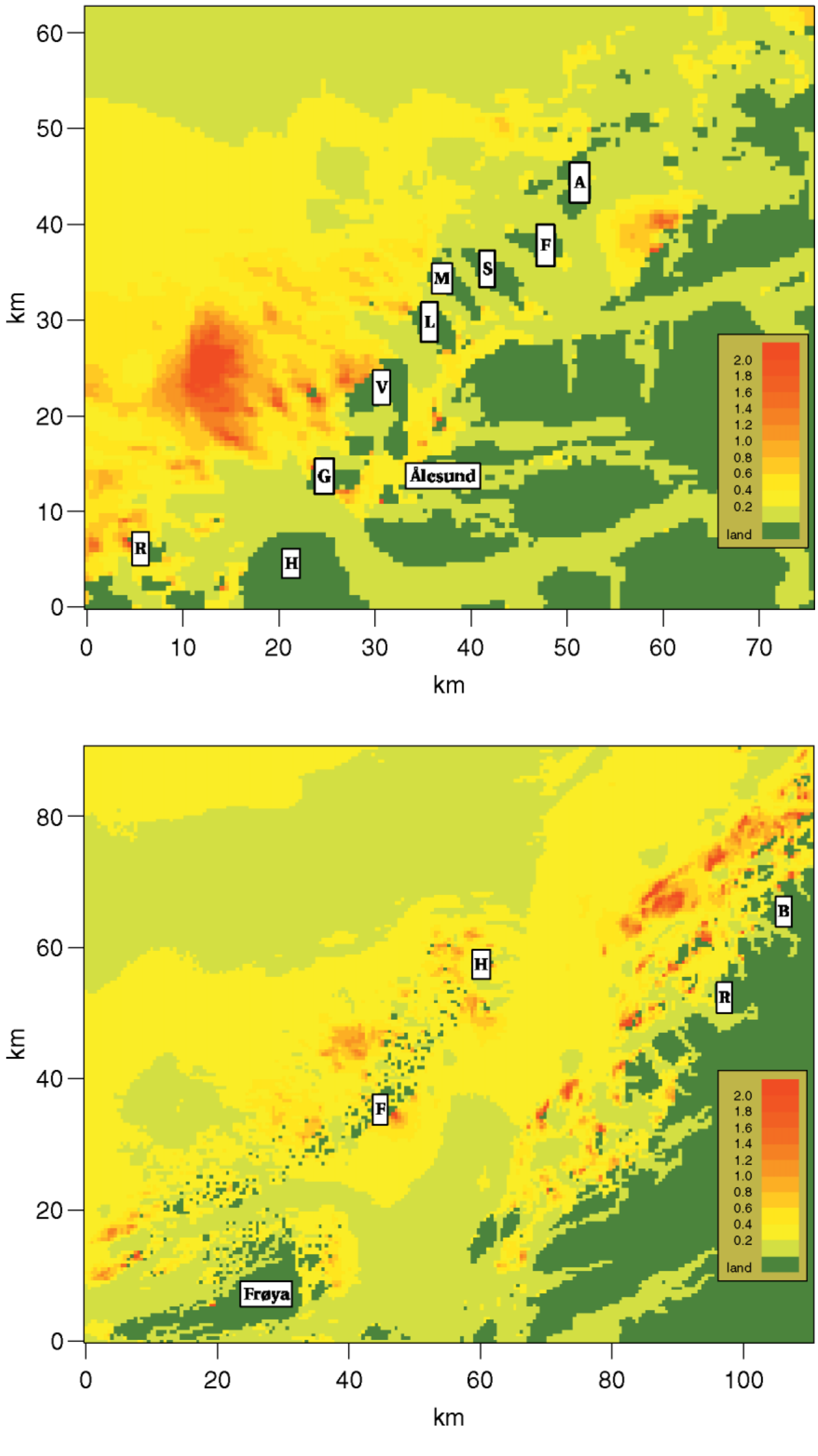

Fig. 9. The ratio between the major axis of the current ellipses for the K_1 and M_2 components for the outer Sunnmøre area (upper panel) and the Froan area (lower panel). Color scale in legend. Map codes, upper panel: H: Hareidlandet, R: Runde, G: Godøya, V: Vigra, L: Løvsøya, M: Haramsøya, S: Skuløya, F: Fjørtoft, A: Harøya. Map codes, lower panel: F: Froan, H: Halten, R: Roan, B: Bessaker.

to the model boundary it may be an artificial effect of the boundary conditions.

A detailed discussion of the tidal currents is limited to three areas: the Ramsøyfjord, between the islands of Smøla and Hitra, with the pipeline to Tjeldbergodden, Trondheimsleia – the most important sailing route, and the outer Sunnmøre, north-west of Ålesund, with diurnal (K_1) current dominance in some locations. Current vector fields plotted in Figs. 10–13 are made with reduced resolution (every third grid point) to avoid cluttering and with no vectors drawn for depths less than 10 m to improve readability.

Ramsøyfjorden. For Ramsøyfjorden and outwards to the Haltenbanken area, there are current observations available

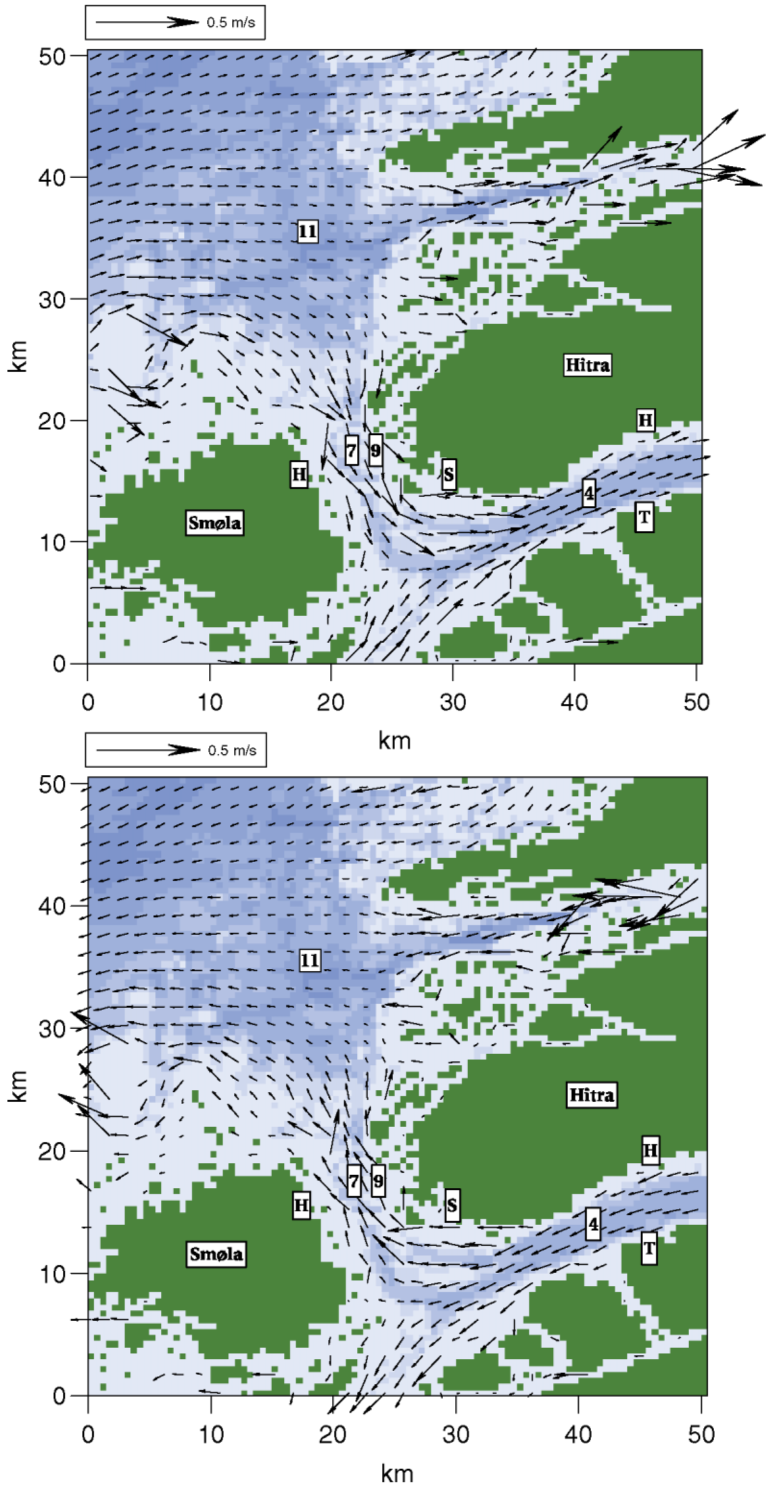

Fig. 10. Upper panel: M_2 current field at the time of peak incoming current in the Ramsøyfjorden area. Lower panel: M_2 current field at the time of peak outgoing current. Map codes: 4 corresponds to St04, 7 to St07, 9 to St09 and 11 to St11. Two cross-sections are also indicated: H-S: Ramsøyfjorden, T-H: Tjeldbergodden.

from several stations which can be used for model validation. The data are presented in Tables 5 and 6, and compared with modeled data from the elevation-driven simulations. For most of the stations along the Tjeldbergodden pipeline (Table 2, St04–St16,) current measurements were made by sensors 3–5 m above the sea bed. When only near-bottom measurements are available a depth mean current is estimated by assuming a boundary layer profile (Schlichting 1979), and used for comparison with model data. The mean current is taken to be $\bar{v} = v_{\mathrm{i}}\left(\frac{h}{\Delta h}\right)^{\frac{1}{10}}$, where $\bar{v}$ is the mean current, v_i the measured current, h the total depth and Δh the height of the current meter above the sea bed. Here, Δh is 3 m for all stations.

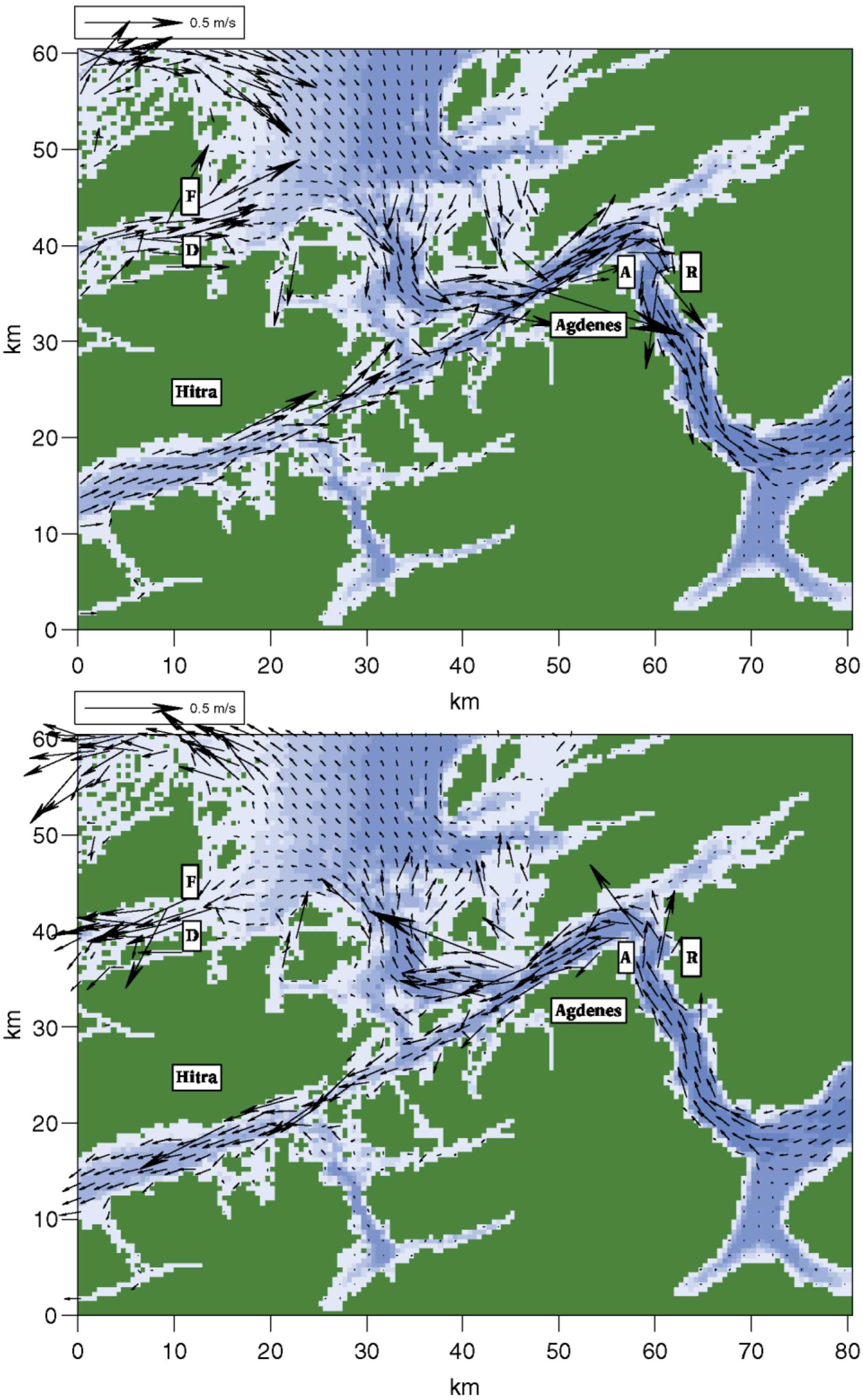

Fig. 11. Upper panel: M_2 current field at the time of peak incoming current in the Trondheimsleia area. Lower panel: M_2 current field at the time of peak outgoing current. Two cross-sections are marked: A-R: Agdenes, D-F: Frøyfjorden.

For station St07 measurements are available for three depths through the water column. Data from 51 m above the sea bed is used, which seemed to be a representative mean value. For the semi-diurnal components the modeled peak currents, represented with the major half axes, are in good agreement with observations for most of the stations. For the the other ellipse parameters, minor half axis, orientation and rotation, the agreement is not so good. The boundary layer approximation made could have contributed to these discrepancies, as could also stratification, local

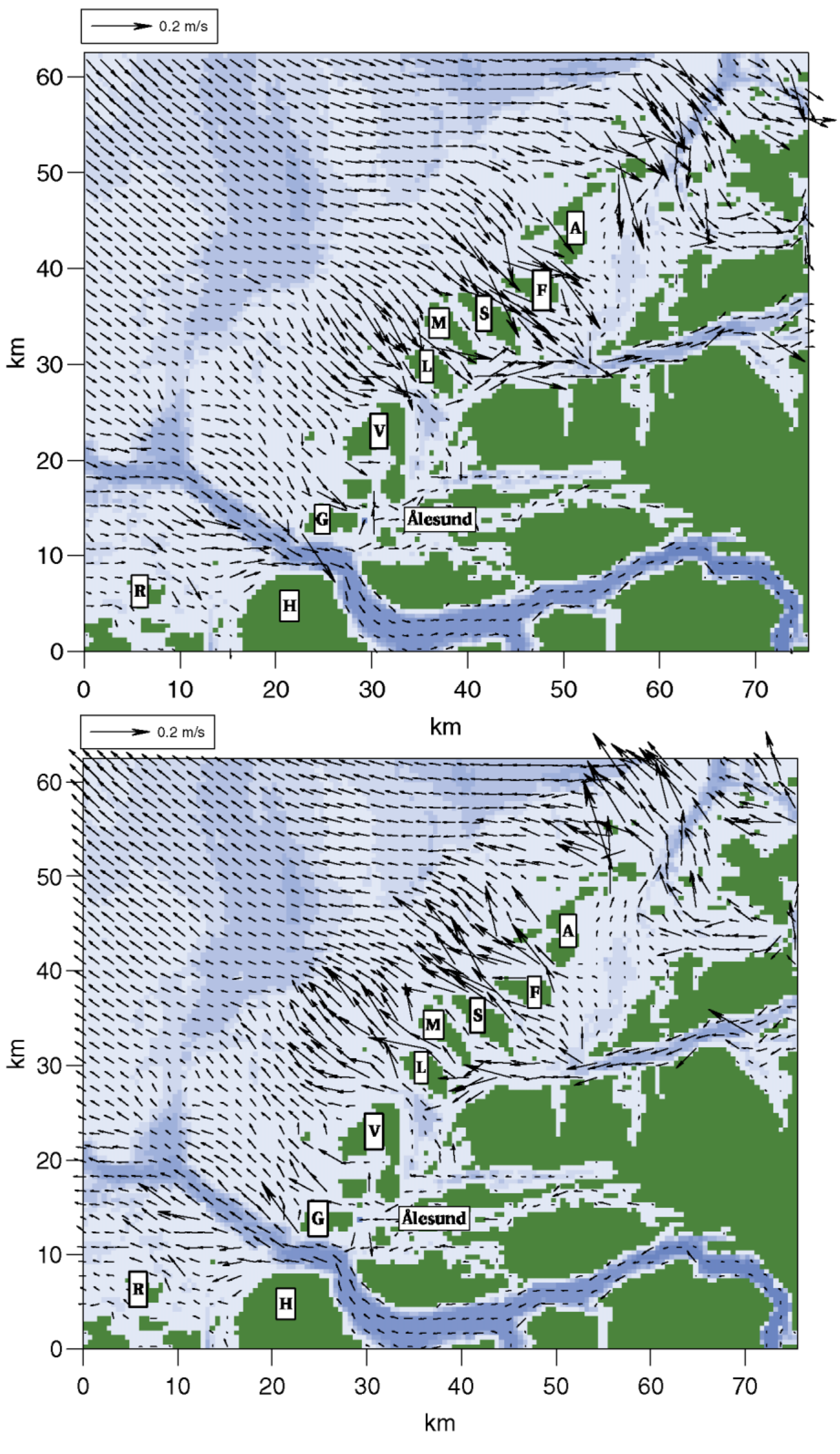

Fig. 12. Upper panel: M_2 current field at the time of peak incoming current in the outer Sunnmøre area. Lower panel: M_2 current field at the time of peak outgoing current. Map codes as in Fig. 9, upper panel.

topographic effects, etc. The diurnal, K_1, peak current is too small for most stations; the model seems to systematically underestimate the diurnal current.

The M_2 current fields at the times of peak incoming and outgoing tidal currents is plotted (Fig. 10). An enlarged plot of the tidal ellipse and rotation for the current vector and the maximum current (major half axis) for M_2 and K_1, for the same area as in Fig. 10, are shown in Moe et al. (2000).

Trondheimsleia. The channel between the island of Hitra and the mainland is called Trondheimsleia (the lead to Trondheim). The long Trondheimsfjord (total length

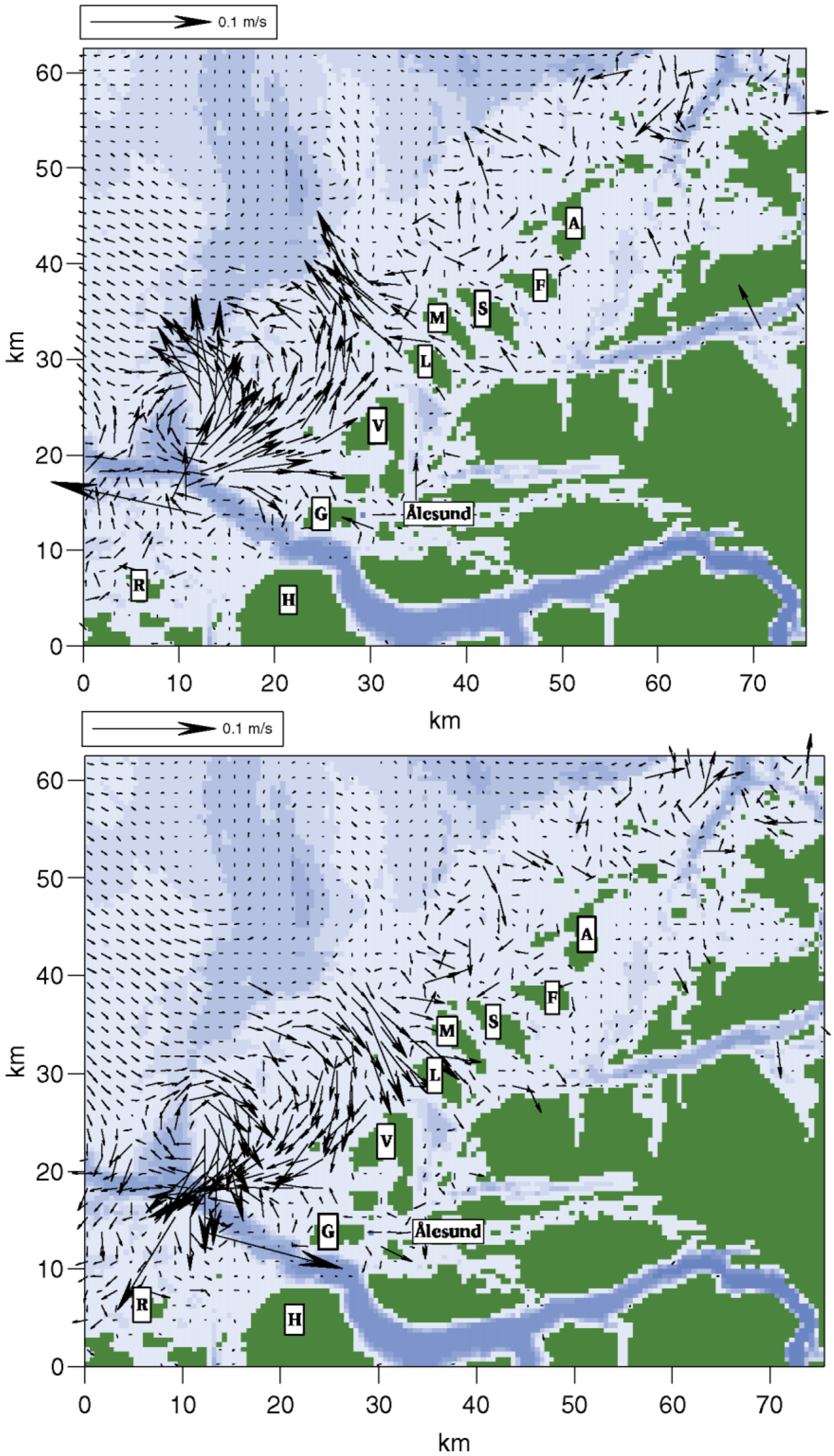

Fig. 13. Upper panel: K_1 current field at the time of peak outgoing current in the outer Sunnmøre area. Lower panel: K_1 current field at the time of peak incoming current. Map codes as in Fig. 9, upper panel.

120 km), stretches from Agdenes at the mouth towards Trondheim and further inwards to Steinkjer (Fig. 2, map code 12). This fjord system is important for ship traffic along the coast. The large surface area of the Trondheimsfjord and the influx from several large rivers imply a large water exchange through the relatively narrow mouth at Agdenes. A study of the circulation and water exchange in the Trondheimsfjord was published by Jacobson (1983). A numerical model of the tide in the fjord inside Agdenes was published by Utnes & Brørs (1993). With the present model, the inner part of the Trondheimsfjord is included as part of a larger model domain, thus avoiding estimates of boundary conditions at Agdenes. Also, the present model has an overall finer grid resolution in the Trondheimsfjord than the

Table 5. Parameters for the M_2 current ellipse. A (cm/s), major half axis; B (cm/s), minor half axis; θ, orientation of major axis in degrees true; Rot., rotation direction for the current vector (+, clockwise; −, counterclockwise). Total depths are included for some of the stations.

Station	*Observed*				*Model*			
(map code)	A	B	θ	Rot.	A	B	θ	Rot.
St04 (230 m)	9.1	1.1	33	−	8.8	0.1	25	+
St07 (151 m)	15.7	0.1	99	+	12.7	1.5	101	+
St09 (75 m)	3.5	2.0	44	−	9.6	0.1	139	−
St11 (300 m)	2.8	1.8	111	−	3.2	0.8	166	−
St13 (275 m)	4.3	2.7	33	−	5.4	0.5	39	−
St15 (257 m)	8.1	0.2	4	−	6.4	0.1	14	+
St16 (219 m)	5.2	0.2	17	−	5.8	2.2	14	−
Draugen	8.5	3.7	359	+	6.7	0.7	6	+
Haltenbanken 1	5.6	0.7	354	+	6.8	1.3	4	+
Haltenbanken 2	10.0	1.7	112	−	6.2	0.4	11	+
Haltenbanken 3	5.3	1.2	185	−	6.5	1.0	6	+
Helland Hansen	4.8	0.9	27	+	4.4	0.3	13	−

Table 6. Parameters for the K_1 Current Ellipse. A (cm/s), major half axis; B (cm/s), minor half axis; θ, orientation of major axis in degrees true; Rot., rotation direction for the current vector (+, clockwise; −, counterclockwise). Total depths are included for some of the stations.

Station	*Observed*				*Model*			
(map code)	A	B	θ	Rot.	A	B	θ	Rot.
St04 (230 m)	0.4	0.1	61	−	0.9	0.0	25	+
St07 (151 m)	1.3	0.1	92	+	0.7	0.1	110	+
St09 (75 m)	2.0	0.1	0	+	0.5	0.0	138	−
St11 (300 m)	1.2	0.2	105	+	0.3	0.0	21	−
St13 (275 m)	1.4	0.2	42	+	1.2	0.3	46	+
St15 (257 m)	1.8	1.0	44	+	1.3	0.3	31	+
St16 (219 m)	3.0	1.9	43	+	1.1	0.8	30	−
Draugen	1.4	0.8	350	+	1.3	0.4	21	+
Helland Hansen	3.2	1.2	179	+	1.3	0.4	178	+

model by Utnes & Brørs. In Fig. 11, the M_2 current fields at the times of peak incoming and outgoing tidal currents are shown for this area. Fig. 11 shows strong currents in the shallower parts of the fjord, particularly in the area near Ørlandet and Storfosna, west of Agdenes, and also substantial currents for the deeper parts of Trondheimsleia and Trondheimsfjorden. Enlarged plots of the tidal ellipse and rotation for the current vector and the maximum current (major half axis) for M_2 and K_1 respectively, for the same area can be found in Moe et al. (2000). The M_2 current dominates over the K_1 current in Trondheimsfjorden.

Volume fluxes through key cross-sections. For some main channels between the larger islands near the entrance to Trondheimsfjorden the peak M_2 volume flux (Q) through cross-sections of the channels have been calculated (Table 7) (Figs. 10 and 11). A mean peak current speed for the cross-sections is calculated and may serve as a more robust measure of the current speed than values from single grid points. The time delay (ΔT) from local high water to peak volume flux is also calculated and the results are displayed in Table 7.

The mean peak current speed in the cross-section in Ramsøyfjorden (Fig. 10, H-S) compares well with the measured major axis of the current ellipse at stations St07 and St09 located near the cross-section (Table 5). The time delay between modeled local high water and peak volume flux in this cross-section is c. 3.5 hours, indicating a standing wave oscillation in this area. Mean peak current speed in the cross-section near Tjeldbergodden (Fig. 10, T-H) is in good agreement with the measurement of the major axis at station St04 (Table 5). In cross-section D-F (Fig. 11), Frøyfjorden, current measurements are available from position 63.40°N, 8.48°E (Mathisen et al. 1997). The mean major axis was measured to 49.8 cm/s, in reasonable agreement with the mean speed in Table 7. Recent current records by *Statoil* (E. Nygaard, personal communication 2002) in the deep channel near Agdenes, near cross-section A-R, show major half axis between 13.0 cm/s and 26.8 cm/s, which compares reasonably well with the mean speed calculated in Table 7.

Outer Sunnmøre. The outer Sunnmøre area is located north-west of Ålesund, one of Norway's largest fishery harbors. An interesting pattern is seen in the current field

Table 7. Peak M_2 volume flux. Area of cross-section S (m^2); Volume flux Q (m^3/s); Mean peak speed $U_s = Q/S$ (cm/s); Time delay ΔT (hours).

Cross-section	S	Q	U_s	ΔT
Ramsøyfjorden (H-S)	$6.3 \cdot 10^5$	$6.1 \cdot 10^4$	9.6	3.5
Tjeldbergodden (T-H)	$9.9 \cdot 10^5$	$7.3 \cdot 10^4$	7.4	4.0
Agdenes (A-R)	$1.5 \cdot 10^6$	$1.8 \cdot 10^5$	12.5	3.1
Frøyfjorden (D-F)	$1.0 \cdot 10^5$	$4.1 \cdot 10^4$	39.8	3.9

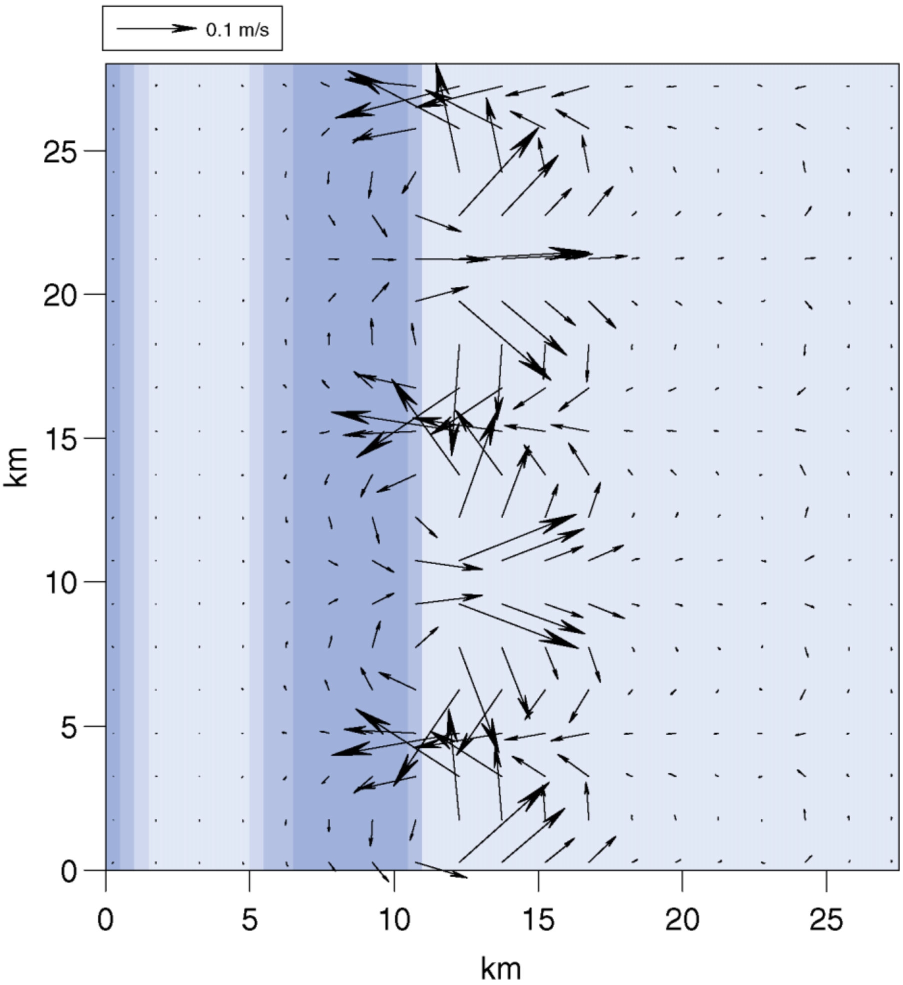

Fig. 14. Current field for a 24-hour period shelf wave for a depth profile along a section from the western part of Vigra (Fig. 12, map code V) westward to the end of the plotting area in Fig. 12. Color code for depth and start of horizontal axis as in Fig. 12.

near Nordøyane, the chain of islands north of Ålesund (Figs. 12 and 13, labels A-G). Figs. 12 and 13 show the current fields at the times of peak incoming and outgoing tidal currents for M_2 and K_1 respectively. Enlarged plots of tidal ellipse and rotation of current vectors for the Sunnmøre area can be found in Moe et al. (2000).

As revealed by Fig. 9 and by visual inspection from the current plots (Figs. 12 and 13), the K_1 current is larger than M_2 west of Vigra. A vortex in the K_1 current pattern west of the islands of Godøya and Vigra and other vortical structures further north are clearly seen. The current direction in the vortices alternate periodically with the diurnal period. The special topographic feature with the fjord ending between Hareidlandet and Godøya and continuing as a trench far into the shelf south of the vortex should be noted. A branch of the trench goes northward to the west of the vortex. Between the island of Vigra and the northern branch of the trench the depth is very shallow. Obviously, the formation of the vortex structure is linked to the bottom topography in the area.

In the northern part of Nordøyane there is a strong M_2 current running in the channels between the islands in interaction with the flow in and out of the wide fjords east of the islands. In this area there is a clear M_2 dominance.

In order to understand the vortex formation in the K_1 current field, the possibility for shelf waves with a 24-hour period associated with the depth profiles outside the island of Vigra has been investigated by a modal analysis. A shelf wave mode with a period of 24 hours is found to be possible for a profile starting off the west coast of Vigra and continuing west to the end of the plotting area (Fig. 12). Fig. 14 shows an idealised bottom topography, with the Vigra depth profile, uniform in the north-south direction, superimposed with the calculated current field for the 24-hour period shelf wave. Although this is a simple model it displays vortex features similar to those in Fig. 13, indicating that the strong K_1 current is due to shelf wave modes associated with the bottom topography near Vigra.

Concluding remarks

The high resolution depth-integrated model is found to reveal important features of the dynamics of the tides outside the coast of Møre and Trøndelag. This large-scale variation in sea level amplitude and phase for the three semi-diurnal constituents M_2, S_2 and N_2 is in good agreement with observations for most of the stations.

The simulations show that the diurnal tidal current dominates in some of the shallow areas on the coast of Sunnmøre and likewise in some of the shallow areas further north: west of Froan, and west of Roan-Bessaker on the coast of Trøndelag. As far as we know, this unexpected result is not documented by measurements and this could therefore be an interesting endeavour for future tidal measurements in the area.

Although the agreement between model and observation is generally very good, systematic deviations are noted, especially for the diurnal component. As indicated by a simple test of the effect of the boundary conditions for the K_1 component, this can be improved by the use of systematic optimalization techniques.

The ability of the model to predict the current along the pipeline from Haltenbanken to Tjeldbergodden shows that the local tidal conditions are to a large extent determined by the large-scale dynamics of the tide in deep water where non-linear effects are negligible. In order to simulate the current field in channels with strong tidal current turbulence, flow separation and eddy formation need to be represented in a more realistic way in the model. This will require use of adaptive grid or nesting of finer grid models in certain areas. Also, particularly at certain times of the year, density stratification may have a considerable effect on the tidal current and therefore needs to be incorporated in the model in order to provide more accurate simulation of currents.

Despite these limitations, the results of the simulations with this barotropic tidal model stand by their own right and could serve as a starting point for more advanced modeling exercises, as well as a guidance for future measurement programs.

A refined model of the tide in Trondheimsleia with 50–100 m grid resolution is in progress as a part of the BeMatA project (http://www.math.uio.no/~bjorng/bemata) funded by the Research Council of Norway. During this project the tidal current field for a test area in Trondheimsleia will be implemented in the new generation of electronic sea charts (ECS). This work is being done in cooperation with the Norwegian Hydrographic Service.

Another possible use of the high resolution tidal current fields is in the aquaculture industry. High resolution current fields can be used for calculation of drift and dispersion of passively floating particles in the flow field (Ommundsen 2002), thus providing methods for estimating risk of spreading of pollutants and infections from one fish farm to another.

Acknowledgements.—The first version of this model with the high resolution matrix was developed and tested under a contract with *Statoil*, which also has provided current and sea level data for model validation.

We are grateful to the Norwegian Hydrographic Service, *Statens Kartverk*, for access to their data archive on sea level and current records. The assistance by O. Høvik and E. Dybesland in generating a high resolution depth matrix for the area is greatly appreciated. This work has also received support from the Research Council of Norway (contract 133102/431, BeMatA program).

Manuscript submitted 1 October 2001; accepted 15 October 2002

References

Davies, A. M., Jones, J. E. & Xing, J. 1997a. Review of recent developments in tidal hydrodynamic modeling. I Spectral models. *Journal of Hydraulic Engineering* 123:4, 278–292.

Davies, A. M., Jones, J. E. & Xing, J. 1997b. Review of recent developments in tidal hydrodynamic modeling. II Turbulence energy models. *Journal of Hydraulic Engineering* 123:4, 293–302.

Davies, A. M., Kwong, S. C. M. & Flather, R. A. 1997c. A three-dimensional mode of diurnal and semidiurnal tides on the European shelf. *Journal of Geophysical Research* 102 (C4), 8625–8656.

Eide, L. I. 1979. Evidence of a topographically trapped vortex on the Norwegian continental shelf. *Deep-Sea Research* 26/6A, 601–621.

Foreman, M. G. G. 1978. *Manual for Tidal Currents Analysis and Prediction*. Pacific Marine Science Report 78-6. Institute of Ocean Sciences , Patricia Bay, Sidney, B.C.

Geyer, W. R. 1993. Three-dimensional tidal flow around headlands. *Journal of Geophysical Research* 98, 1, 955–966.

Gjevik, B. 1990. Model simulations of tides and shelf waves along the shelves of the Norwegian-Greenland-Barents Seas. Davies, A. M. (ed.) *Modelling Marine Systems* 1, 187–219. CRC Press Inc, Boca Raton, Florida.

Gjevik, B. & Straume, T. 1989. Model simulations of the M_2 and the K_1 tide in the Nordic Seas and the Artic Ocean. *Tellus* 41A, 73–96.

Gjevik, B. & Moe, H. 1994. Steady and transient flows around a bank located near a shelf edge. *Continental Shelf Research* 24, 1389–1409.

Gjevik, B., Nøst, E. & Straume, T. 1990. *Atlas of Tides on the Shelves of the Norwegian and the Barents Seas*. Report FoU-ST 90012. Department of Mathematics, University of Oslo , Oslo.

Gjevik, B., Høvik, O. & Moe, H. 1992. *Simulering av tidevannet i kystområdet innenfor Haltenbanken*. Rapport TJ-92-1 [for *Statoil*]. Matematisk institutt, Universitetet i Oslo , Oslo. 39 pp.

Gjevik, B., Nøst, E. & Straume, T. 1994. Model simulations of the tides in the Barents Sea. *Journal of Geophysical Research* 99, (C2), 3337–3350.

Haugan, P. M., Evensen, G., Johannessen, J. A., Johannessen, O. M. & Pettersson, L. H. 1991. Modeled and observed mesoscale circulation and wave-current refraction during the 1988 Norwegian continental shelf experiment. *Journal of Geophysical Research* 96 (C6), 10,487–10,506.

Jacobson, P. 1983. Physical oceanography of the Trondheimsfjord. *Geophysical and Astrophysical Fluid Dynamics* 26, 3–26.

Maddock, L. & Pingree, R. D. 1978. Numerical simulation of the Portland tidal eddies. *Estuarine and Coastal Marine Science* 6, 353–363.

Martinsen, E. A. & Engedahl, H. 1987. Implementation and testing of a lateral boundary scheme as an open boundary condition in a barotropic ocean model. *Coastal Engineering* 11, 603–627.

Martinsen, E. A., Gjevik, B. & Røed, L. P. 1979. A numerical model for long barotropic waves and storm surges along the western coast of Norway. *Journal of Physical Oceanography* 9:6, 1126–1138.

Mathisen, J.-P. 1998. *Deep Water Current Measurements. Final Report*. Report OCN R-98007. Oceanor, Trondheim.

Mathisen, J.-P., Arff, J. & Stokland, Ø. 1997. *Vurdering av miljøkonsekvensene som følge av bruforbindelse over Frøyafjorden*. Report OCN R-96046. Oceanor, Trondheim.

Mesinger, F. & Arakawa, A. 1976. *Numerical Methods Used in Atmospheric Models*. GARP Publication Series No. 17. World Meteorological Organization , Geneva, Switzerland. 64 pp.

Moe, H., Gjevik, B. & Ommundsen, A. 2000. *A High Resolution Tidal Model for the Coast of Møre and Trøndelag, Mid Norway*. Report, Department of Mathematics, University of Oslo , Oslo.

Moe, H., Ommundsen, A. & Gjevik, B. 2002. A high resolution tidal model for the area around the Lofoten Islands, Northern Norway. *Continental Shelf Research* 22, 485–504.

Nøst, E. 1988. Simulering av tidevann på Haltenbanken. Master's thesis, University of Oslo. 110 pp.

Norwegian Hydrographic Service 1992. *OKN-Thematic Map Offshore Mid-Norway. Stavanger, Norway*. Norwegian Hydrographic Service , Stavanger.

Norwegian Hydrographic Service 2000. *Tide Tables for the Norwegian Coast and Svalbard*. Norwegian Hydrographic Service , Stavanger.

Ommundsen, A. 2002. Models of cross shelf transport introduced by the Lofoten Maelstrom. *Continental Shelf Research* 22:1, 93–113.

Orvik, K. A., Skagseth, O. & Mork, M. 2001. Atlantic inflow to the

Norwegian Seas: current structure and volume fluxes from moored current meters, VM-ADCP and SeaSoar-CTD observations, 1995–1999. *Deep Sea Research* 48:1, 937–957.

Poulain, P.-M., Warn-Varnas, A. & Niiler, P. P. 1996. Near-surface circulation of the Nordic Seas as measured by Lagrangian drifters. *Journal of Geophysical Research* 101 (C8), 18,237–18,258.

Sætre, R. 1999. Features of the central Norwegian shelf circulation. *Continental Shelf Research* 19, 1809–1831.

Schlichting, H. 1979. *Boundary Layer Theory*. McGraw-Hill Book Company , New York.

Schwiderski, E. W. 1980. On charting global ocean tides. *Reviews of Geophysics* 18, 243–268.

Utnes, T. & Brørs, B. 1993. Numerical modelling of 3-D circulation in restricted waters. *Applied Mathematical Modelling* 17, 522–535.